Precision Molecular Engineering of Compact Near-Infrared Fluorophores

Precision Molecular Engineering of Compact Near-Infrared Fluorophores

Rongrong Huang,[#1,2] Qinglong Qiao,[#3] Deborah Seah,[4] Tianruo Shen,[1] Xia Wu,[1] Fabio de Moliner,[4] Chao Wang,[1] Nannan Ding,[2] Weijie Chi,[5] Huaming Sun,[2] Marc Vendrell,*[4] Zhaochao Xu,*[3] Yu Fang,*[2] Xiaogang Liu*[1]

[#]These authors contributed equally to this work.

[1]Fluorescence Research Group, Singapore University of Technology and Design, 8 Somapah Road, Singapore 487372 (Singapore). E-mail: xiaogang_liu@sutd.edu.sg

[2]Key Laboratory of Applied Surface and Colloid Chemistry (Ministry of Education), School of Chemistry and Chemical Engineering, Shaanxi Normal University, Xi'an, Shaanxi 710119 (P. R. China). E-mail: yfang@snnu.edu.cn

[3]CAS Key Laboratory of Separation Science for Analytical Chemistry, Dalian Institute of Chemical Physics, Chinese Academy of Sciences, 457 Zhongshan Road, Dalian 116023 (P. R. China). E-mail: zcxu@dicp.ac.cn

[4]Centre for Inflammation Research, The University of Edinburgh, EH16 4UU Edinburgh (the United Kingdom); IRR Chemistry Hub, Institute for Regeneration and Repair, The University of Edinburgh, EH16 4UU Edinburgh (the United Kingdom). E-mail: marc.vendrell@ed.ac.uk

[5]Collaborative Innovation Center of One Health, School of Chemistry and Chemical Engineering, Hainan University, Haikou, Hainan 570228 (P. R. China)

ABSTRACT: Organic fluorophores with near-infrared (NIR) emission and reduced molecular size are crucial for advancing bioimaging and biosensing technologies. Traditional methods, such as conjugation expansion and heteroatom engineering, often fail to reduce fluorophore size without sacrificing NIR emission properties. Addressing this challenge, our study utilized quantum chemical calculations and structure-property relationship analysis to establish an iterative design approach and enable precision engineering for compact, single-benzene-based NIR fluorophores. These newly developed fluorophores exhibit emissions up to 759 nm and maintain molecular weights as low as 192 g/mol, approximately 50% of that of Cy7. Additionally, they display unique environmental sensitivity—non-emissive in aqueous solutions but highly emissive in lipid environments. This property significantly enhances their utility in wash-free imaging of live cells. Our findings mark a substantial breakthrough in fluorophore engineering, paving the way for more efficient and adaptable imaging methodologies.

INTRODUCTION

Organic fluorophores have garnered growing interest due to their expansive and promising applications in life sciences and biomedical research (*i.e.*, disease diagnosis, protein quantification, and the study of cellular/organism dynamics).[1-3] In these applications, the efficient diffusion of fluorophores and their tight binding to target biomolecules are crucial.[4, 5] To this end, small molecular size is advantageous in improving cell penetrability and minimizing interference with target biomolecules;[6, 7] smaller molecules also contribute to enhanced imaging resolution in advanced super-resolution microscopy.[8, 9] Besides small molecular sizes, the red and near-infrared (NIR) emissions are highly favored in bioimaging as they enhance penetration depth, reduce auto-fluorescence, and mitigate phototoxicity to cells.[10-13] Developing small and red/NIR (SR) fluorophores is urgently demanded but remains a significant challenge.

Significant efforts have been made to develop red and NIR fluorophores (**Scheme 1a**).[14-16] One established approach for achieving red or NIR emission involves expanding the π-conjugation of a fluorophore. For example, extending the polymethine chain of cyanine dyes can effectively shift their emission wavelengths into the NIR region.[16, 17] Enhancing intramolecular charge transfer (ICT) provides one alternative route to achieve red/NIR emission.[18, 19] By increasing the donor/acceptor strengths, Suzuki and colleagues developed Keio-BODIPYs with emissions spanning the visible to NIR region.[20] Heteroatom engineering presents another promising avenue for realizing bathochromic shifts. For instance, replacing the oxygen-bridging atom in the xanthene scaffold with different heteroatoms, such as sulfur (S), silicon (Si), and phosphorus (P), has resulted in a diverse spectrum of colorful rhodamines with emissions covering the visible to NIR range.[9, 21-23] Using the same strategy, Vendrell et al. developed nitrobenzoxadiazole (NBD)-like SCOTfluor emitting in the visible-to-NIR region.[24]

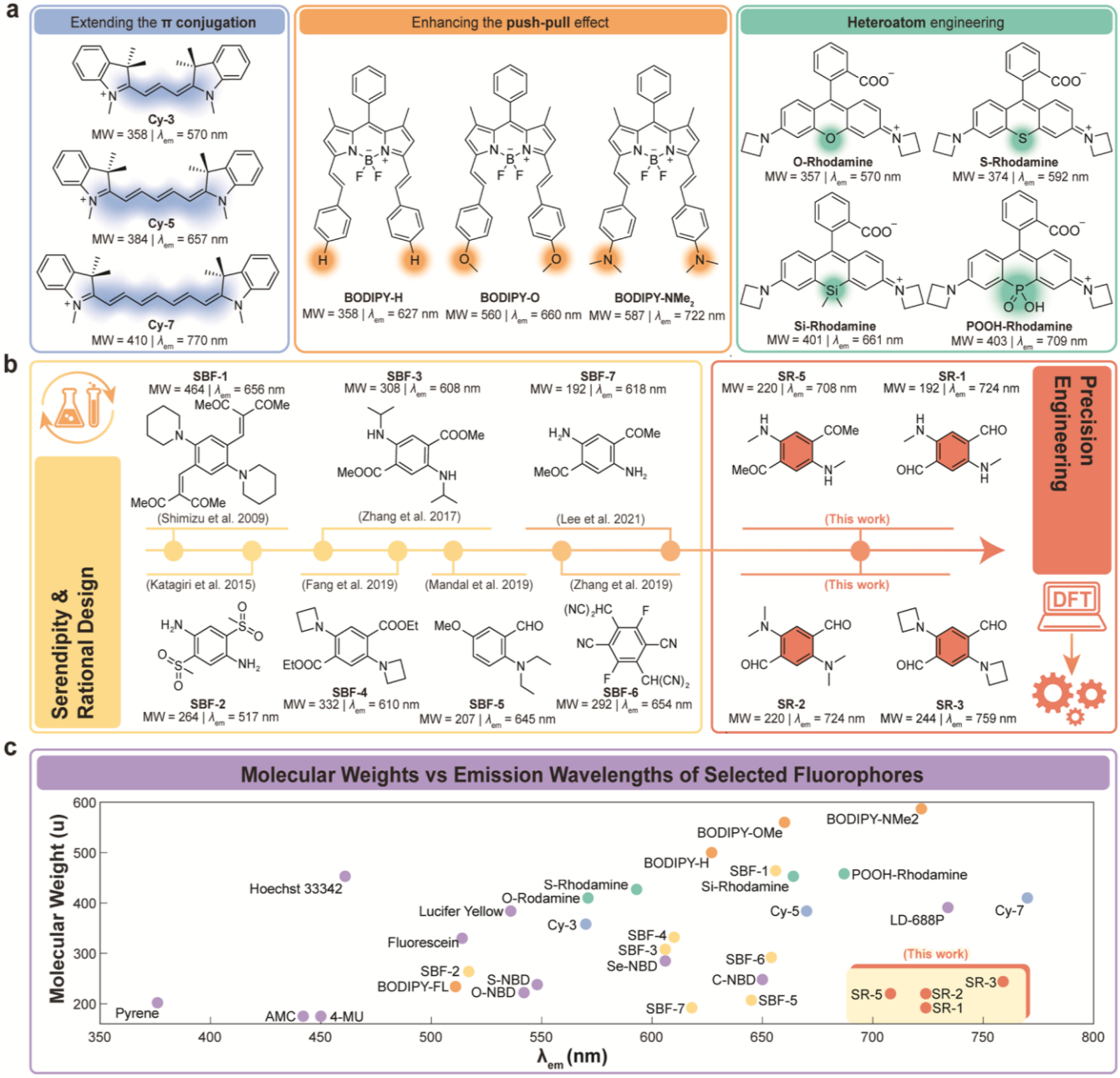

Scheme 1. Schematic representation for developing red/NIR fluorophores and single-benzene fluorophores. a, Popular strategies to develop red and NIR fluorophores and the corresponding chemical structures, molecular weight (MW) and peak emission wavelengths (λ_{em}) of the representative compounds. **b**, Chemical structures, MW, and λ_{em} of the selected single-benzene-based fluorophores. The units of MW and λ are g mol^{-1} and nm, respectively. **c**, A comparison of representative fluorophores' molecular weights vs. peak emission wavelengths.

However, many of these classical fluorophores are characterized by substantial molecular sizes with large and rigid conjugated systems, which may disrupt metabolite traffic and impact protein and enzyme function.[3, 25] In fact, red/NIR emissions and small molecular sizes usually contradict each other as a fluorophore with small conjugation typically has a large electronic gap, resulting in short emission wavelengths.[7, 26] Additionally, many of these fluorophores, including many rhodamine and cyanine dyes, carry a net charge, leading to potential issues such as nonspecific binding to biomolecules.

A unique approach to synthesizing SR fluorophores involves attaching single or multiple donors and acceptors to a single phenyl ring (**Scheme 1b**).[27-31] Shimizu and colleagues made a significant contribution to this field by developing a series of single benzene-based fluorophores,[32] achieving peak emission wavelengths (λ_{em}) up to 656 nm (in cyclohexane; molecular weight (MW) = 465 g/mol). Katagiri and co-workers later synthesized the first benzene-based fluorophore with a molecular weight under 300 g/mol,[33] while preserving green fluorescence (λ_{em} = 517 nm in water). This field was further advanced by Mandal,[34] Fang[35] and Zhang[29, 36] et al., who extended the peak emission

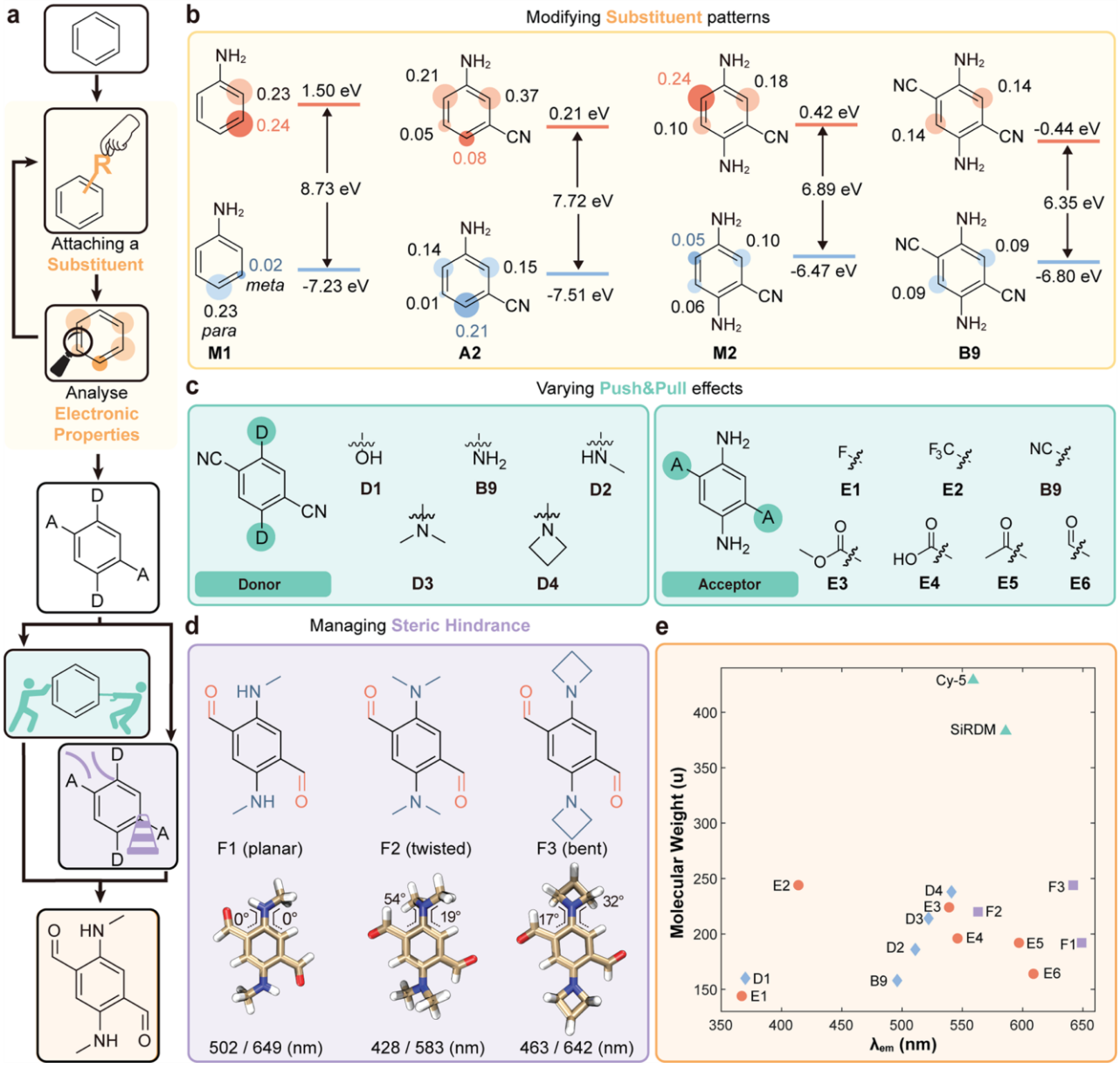

Figure 1. Iterative precision molecular engineering of small and red/NIR fluorophores. a, Schematic illustration of the precision engineering for designing single benzene-based SR fluorophores. **b**, The atomic contributions to HOMO and LUMO of single benzene-based molecules, and the calculated HOMO/LUMO energy levels and corresponding electronic gaps. The calculations are based on the optimized S_1 structures in DMSO. Blue: atomic contributions to HOMO; Red: atomic contributions to LUMO. The numbers in color highlight the substitution positions with significant changes in atomic contributions. **c**, Chemical structures of single benzene-based fluorophores with different donor and acceptor fragments. **d**, Chemical structures of F series with various donors and a -CHO acceptor, their optimized ground-state (S_0) structures, and the calculated peak UV-vis absorption and emission wavelengths. **e**, Calculated peak emission wavelengths vs. molecular weights of single-benzene fluorophores and Cy-5 and Si-rhodamine (SiRDM). Note: the calculations were performed at the ωB97XD/Def2SVP level in DMSO.

wavelengths of single-benzene-based fluorophores to >600 nm, while maintaining molecular weights under 350 g/mol. Additionally, Lee et al. serendipitously developed a red fluorophore *p*-DAPA,[37] characterized by its minimal size (λ_{em} = 618 nm; MW = 192 g/mol). However, the peak emission wavelengths of these compact fluorophores are predominantly confined to the visible spectrum (< 700 nm), and their practical applications have yet to be fully explored. More critically, precise molecular design principles to steer the systematic engineering of SR fluorophores remain undeveloped.

In this study, we leveraged quantum chemical calculations and in-depth structure-property relationship analysis to establish an iterative design approach (**Fig. 1**) and precisely design NIR dyes of minimal sizes (λ_{em} of up to 759 nm in ethanol; MW as low as 192 g/mol; **Scheme 1c**). We systematically identified various factors influencing the spectral properties of these dyes, including substituent positional

effects (**Figs. 1a, 1b**), push-pull dynamics (**Fig. 1c**), and the impact of steric hindrance (**Fig. 1d**), illuminating pathways for precision molecular engineering of SR fluorophores. Notably, the fluorophores developed through this method exhibit outstanding environmental sensitivities and fluorogenicity, facilitating wash-free super-resolution imaging of lipid droplets in live cells and bacterial growth.

RESULTS AND DISCUSSION

Precision engineering of single benzene-based NIR scaffold

Our study established an iterative fluorophore design method guided by quantum chemical calculations (**Fig. 1a**). In the first stage of this method, we introduced substituents sequentially and analyzed the charge density of the frontier molecular orbitals after each substitution. This analysis guided the selection of the next substituent—either donor (D) or acceptor (A)—and determined the precise substitution position on the benzene moiety (**Fig. 1b**). This iterative approach allowed us to strategically place substituents in the most critical positions, thereby maximizing the bathochromic shift while maintaining minimal molecular sizes.

Specifically, after installing one donor group (i.e., D = -NH_2), we observed minimal electron density in the highest occupied molecular orbital (HOMO) and a high density in the lowest unoccupied molecular orbital (LUMO) at the *meta*-position of the 1D-substituted compound M1 (**Fig. 1b**). Therefore, placing an acceptor (i.e., A = -CN) at this *meta*-position to the donor in M1 would significantly stabilize and lower the LUMO with minimal impact in the HOMO, reducing the electronic gap and leading to significant bathochromic shifts. This shift was exemplified in the 1D-1A compound A2, where the acceptor is at the *meta*-position to the donor, yielding a much lower electronic gap. Similarly, at the *para*-position of M1 and A2, the electron density is notable in the HOMO but significantly reduces in the LUMO. This difference suggests that adding a donor at the *para*-position would raise and destabilize the HOMO while minimally affecting the LUMO.[38, 39] The resulting redshift is evidenced by the significant reduction of the electron gap from A2 (7.72 eV) to M2 (6.89 eV). Similarly, by observing the charge density of M2, we found that the most effective redshift was achieved by combining two pairs of donors and acceptors in B9 (6.35 eV): two D fragments are positioned *para* to each other (as were the acceptors). Additionally, each A fragment is positioned *meta* to a D fragment.

We opted not to introduce additional substituents to B9. This is due to the potential for significant scaffold distortion in heavily substituted benzene rings, particularly with larger donor/acceptor (D/A) fragments (such as azetidine and -CHO). This distortion due to steric hindrance can lead to non-emissive states.

We have substantiated the effective substitution pattern of B9 through exhaustive computational screening. We explored various donor-acceptor ratios in three series: 1:1 (A series; Fig. S1a), 2:2 (B series; Fig. S1b), and 3:3 (C series; Fig. 1c), attaching D/A groups at different positions on the benzene scaffold. Our computational screening validated that the B9 emerged as the ideal candidate for further *in silico* molecular engineering, demonstrating the effectiveness of the iterative design approach (Fig. S1d).

The substitution pattern of B9 closely resembles that of several previously reported small, red, single-benzene fluorophores (**Scheme 1b**). However, this study is the first to rationalize this pattern using a bottom-up approach, employing iterative precision engineering guided by quantum chemical calculations.

In silico molecular engineering of the single benzene-based NIR fluorophores

Guided by the substitution pattern in B9, the second stage of the iterative design method focused on the impact of varying the electron-donating and -accepting strength of the D/A fragments on the λ_{abs} and λ_{em} of benzene-based SR fluorophores (**Fig. 1c**). By retaining -CN as the acceptor, an increase in the electron-donating strength of the donor from -OH to azetidine generally resulted in a red-shifted λ_{em} from 370 nm to 541 nm (**Figs. 1c**, **1e**). Similarly, maintaining -NH_2 as the donor, a progressive increase in the electron-withdrawing strength of the acceptor from -F to -CHO led to a bathochromic shift from 367 to 609 nm. These findings underscore that enhanced charge transfer can significantly amplify the bathochromic shifts.

Steric hindrance also plays a pivotal role in influencing the redshifts of λ_{abs} and λ_{em} by impacting the planarity (and the conjugation) of the fluorophore. This effect is also addressed and optimized in the second stage of the design process. For example, when opting for the aldehyde group as the acceptor (F series; **Fig. 1d**), the methylamine donor (F1) induces the most significant redshift. However, stronger donors like dimethylamine (F2) and azetidine (F3) result in blue shifts compared to F1. A detailed analysis of the optimized ground state geometries reveals that the D fragments in F2 and F3 exhibit pre-twisted or bent structures due to strong steric repulsion with the aldehyde acceptor. This non-planarity hinders effective charge delocalization, contributing to the blue shift in F2 and F3 compared to F1. In contrast, the methylamine-substituted F1, due to lesser steric hindrance and the formation of an intramolecular hydrogen bond, maintains excellent planarity, emerging as a promising candidate for SR fluorophores.

This thorough structure-property relationship study of single-benzene fluorophores inspired the design of a series of SR fluorophores by enhancing the push-pull effect while managing steric hindrance (**Fig. 1a**). Notably, although quantum chemical calculations often display systematic deviations from experimental data, several candidates, such as F1 and F3 (**Figs. 1d**, **1e**), exhibit longer calculated peak emission wavelengths than popular NIR fluorophores like Cy5 and Si-Rhodamine (Fig. S11). However, the sizes of the SR fluorophores, in terms of molecular weight, are significantly smaller than those of Cy5 and Si-Rhodamine.

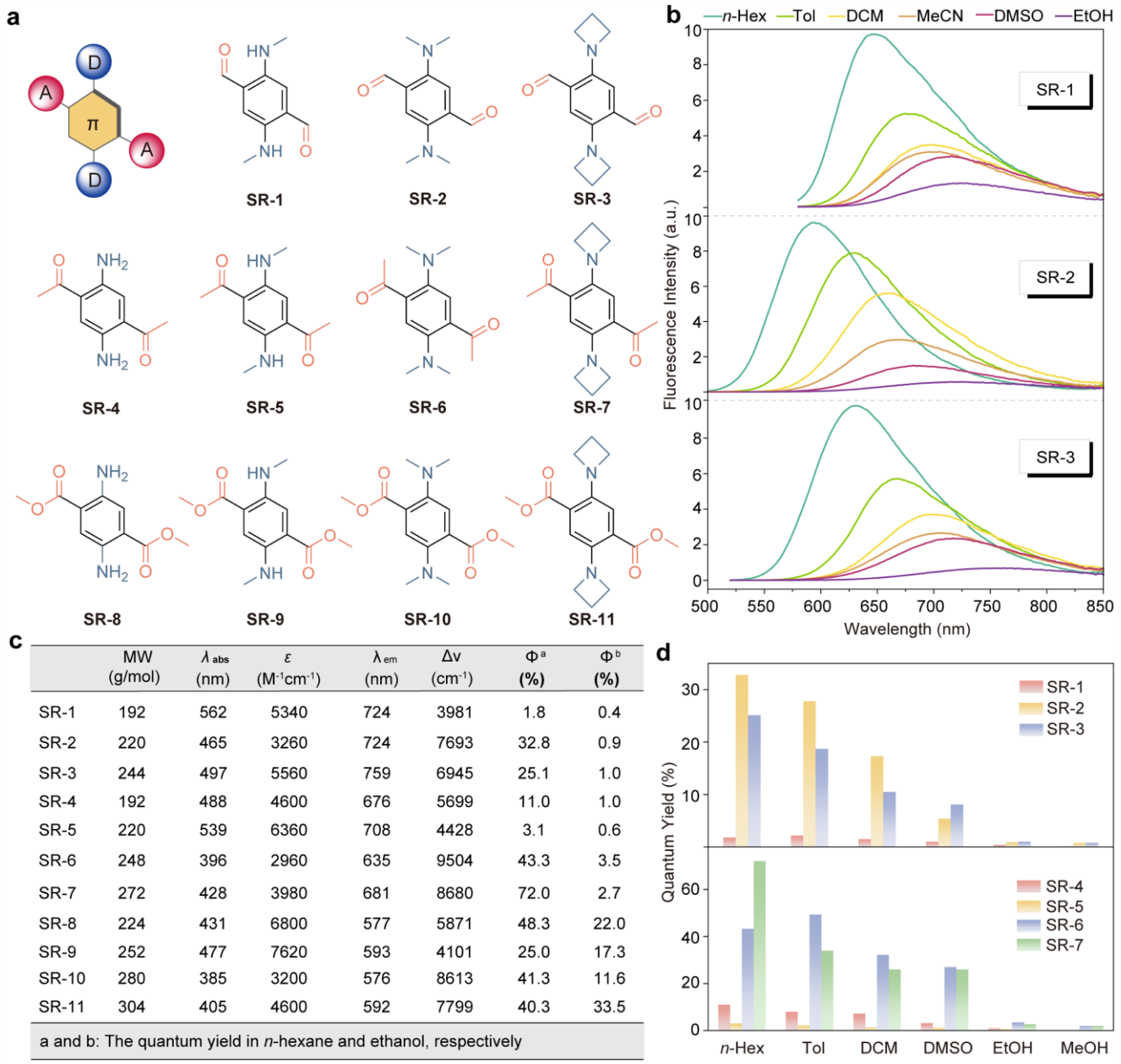

c

	MW (g/mol)	λ_{abs} (nm)	ε ($M^{-1}cm^{-1}$)	λ_{em} (nm)	Δv (cm^{-1})	Φ^a (%)	Φ^b (%)
SR-1	192	562	5340	724	3981	1.8	0.4
SR-2	220	465	3260	724	7693	32.8	0.9
SR-3	244	497	5560	759	6945	25.1	1.0
SR-4	192	488	4600	676	5699	11.0	1.0
SR-5	220	539	6360	708	4428	3.1	0.6
SR-6	248	396	2960	635	9504	43.3	3.5
SR-7	272	428	3980	681	8680	72.0	2.7
SR-8	224	431	6800	577	5871	48.3	22.0
SR-9	252	477	7620	593	4101	25.0	17.3
SR-10	280	385	3200	576	8613	41.3	11.6
SR-11	304	405	4600	592	7799	40.3	33.5

a and b: The quantum yield in *n*-hexane and ethanol, respectively

Figure 2. Photophysical properties of SR fluorophores. a, Chemical structures of SR fluorophores. **b,** Emission spectra of SR-1, SR-2, and SR-3 in different solvents. **c,** The photophysical properties of SR fluorophores. **d,** Fluorescence quantum yields of SR-1, SR-2, SR-3, SR-4, SR-5, SR-6 and SR-7 in different solvents. The concentrations of the samples are 50 μM.

Chemical synthesis, structure, and spectral characterization

Building on the trend and insights from our theoretical analysis, 11 single-benzene fluorophores were designed and synthesized (**Fig. 2a**, Figs. S12-44). These compounds include our predicted compact NIR fluorophores SR-1 (F1) and SR-3 (F3) and their close derivatives SR-2 and SR-5 to SR-7. Additionally, this set contains derivatives with weaker donors (e.g., SR-4, SR-8) and weaker acceptors (e.g., SR-9 to SR-11). In agreement with theoretical modeling, the crystallography data revealed that the methylamino-substituted SR-5 maintains excellent planarity, forming an intramolecular hydrogen bond between the methylamino and acetyl groups. In contrast, significant pretwisting was observed in the dimethylamino group, with the dihedral angles reaching approximately 69° and 59° for SR-2 and SR-6, respectively (Fig. S45). These findings underscore the importance of managing steric hindrance to preserve the planarity of fluorophores.

Subsequent spectral measurements of these compounds in solvents of varying polarity (**Fig 2b**, Figs. S46-51) revealed that SR-1, SR-2, SR-3, and SR-5 exhibited NIR emissions, respectively peaking at 724, 724, 759, and 708 nm in ethanol (**Fig. 2c**). In CH_2Cl_2, a weakly polar solvent, the peak emission wavelengths of our predicted SR-1 and SR-3 are 698 nm and 699 nm, respectively. In contrast, reference compounds with weaker donor/acceptor groups emit primarily within the visible spectrum.

We compared the λ_{em} of these single-benzene fluorophores and their molecular weights (**Scheme 1c**, Fig. S52) with

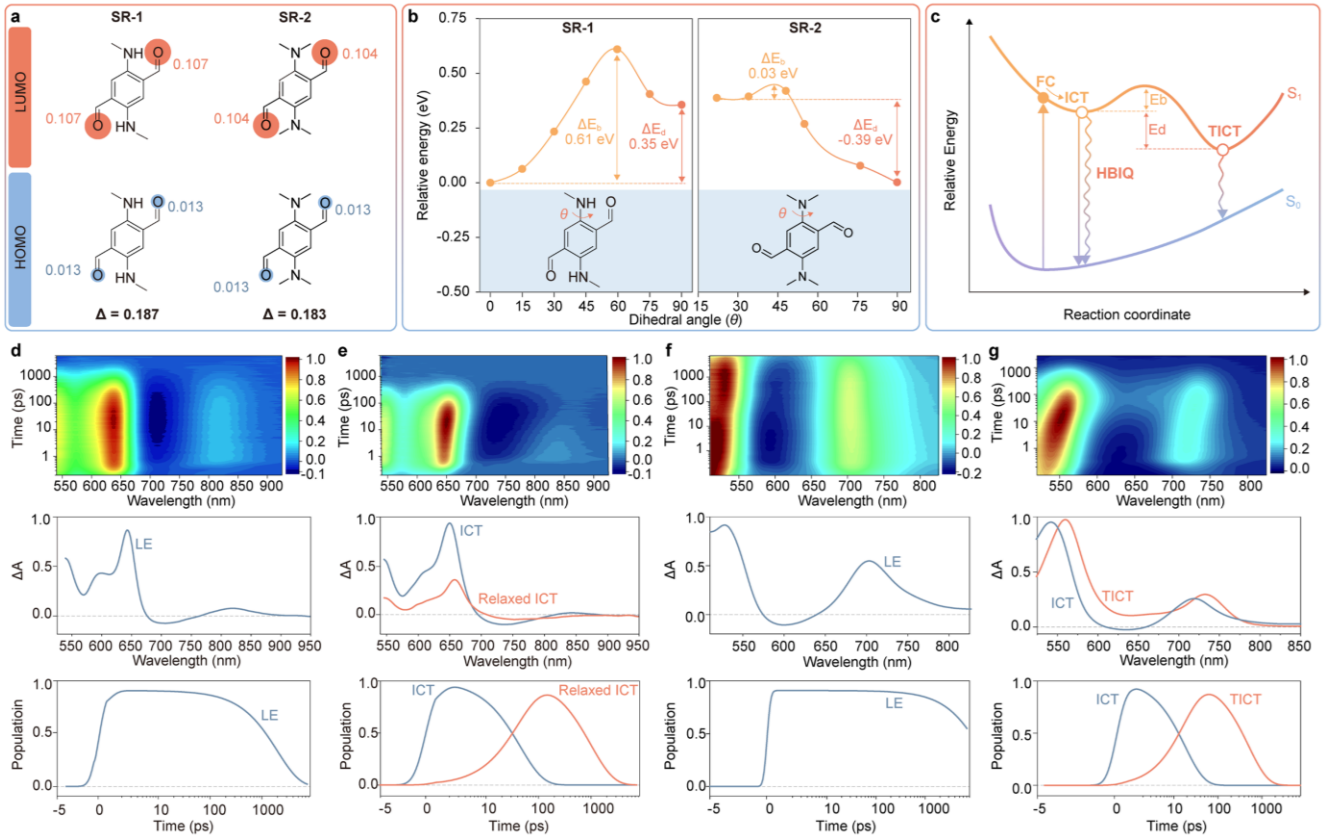

Figure 3. **Excited-state photophysical studies. a**, Atomic contributions to the HOMO and LUMO of SR-1 and SR-2 calculated based on the optimized S_0 structure in DMSO. Blue: atomic contribution to HOMO; red: atomic contribution to LUMO. Δ represents the sum of the absolute change of atomic contributions of HOMO and LUMO at each hydrogen bond accepting site (highlighted in blue and red). **b**, The relative electronic energy of the S_1 potential energy surfaces of SR-1 (left) and SR-2 (right) as a function of dihedral angle θ. Insets show the chemical structures, the dihedral angle (θ), the energy barrier (ΔE_b), and driving energy (ΔE_d) to enter their corresponding TICT states. All calculations were performed at the ωB97XD/Def2SVP level of theory in DMSO. **c**, The proposed mechanism scheme of the SR fluorophores illustrates the energy barrier to enter the TICT state, as well as the radiative and non-radiative decay pathway in polar protic solvents; primary fluorescence quenching channels include hydrogen bond induced quenching (HBIQ) and TICT. **d**, **e**, Transition absorption data of SR-1 pumped at 535 nm in n-hexane (**d**) and ethanol (**e**). **f**, **g**, Transition absorption data of SR-2 pumped at 450 nm in n-hexane (**f**) and ethanol (**g**). The top panel: TA contour; the middle panel: species-associated spectra plots; the bottom panel: relative population profiles of the excited state species.

those of popular NIR fluorophores and previously reported single benzene-based fluorophores (**Scheme 1c**, Fig. S53). Our analysis suggests that SR-1 (or F1) is likely the smallest NIR dye reported to date. This data aligns well with our theoretical predictions.

Due to intense intramolecular charge transfer, these compounds showed significant solvatochromism (**Fig. 2b**, Figs. S49-51 and Table S1). For example, the λ_{em} of SR-3 shifted from 631 nm in *n*-hexane to 759 nm in ethanol (**Fig. 2b**), illustrating the impact of the solvent environment on the spectral properties of these fluorophores. Compared to other solvents, these SR dyes exhibit lower solubility in water, requiring a reduced concentration when preparing aqueous samples.

Molecular origins of environmental sensitivity

We observed not only favorable red/NIR emissions but also significant environmental sensitivity in the quantum yields of the single benzene fluorophores (*i.e.*, SR-1, SR-2, SR-3, SR-4, SR-5, SR-6, SR-7; **Figs. 2c**, **2d**). This environmental sensitivity is attributable to several mechanisms, including hydrogen bond-induced quenching[40] and twisted intramolecular charge transfer (TICT).[41]

Hydrogen bonding interactions with solvent molecules profoundly influence the fluorescence of these single-benzene fluorophores. For instance, SR-3 exhibits moderate fluorescence in aprotic solvents (quantum yield φ = 8% in DMSO) but is non-emissive in protic solvents like ethanol or methanol (**Fig. 2d**, Table S1). To predict the fluorophore's quantum yield susceptibility to hydrogen bond-induced quenching in protic solvents, we have developed a descriptor, Δ.[41] Δ quantifies the absolute change in charge density at the hydrogen bond-accepting site of a fluorophore during the HOMO-LUMO transition, serving as a straightforward descriptor for assessing hydrogen bond sensitivity. A considerable Δ value indicates that photoexcitation significantly perturbs the hydrogen bond equilibrium established in the ground state. In SR fluorophores, this effect is amplified due to intramolecular charge transfer, which increases the charge density at the hydrogen bond-accepting sites. This

enhancement strengthens hydrogen bond interactions with protic solvents in the excited state. The resulting perturbation induces substantial vibrations between the dye and the surrounding solvent as the system re-establishes its hydrogen bond equilibrium in the excited state. Hence, a large Δ suggests substantial vulnerability of quantum yields to hydrogen bond-induced quenching, resulting in lower quantum yields in protic solvents. Our findings show that most of these fluorophores display large Δ values (ranging from 0.17 to 0.21; **Fig. 3a**, Figs. S57-59), indicating lower quantum yields in protic than in aprotic solvents.

In addition to intermolecular hydrogen bond interactions, intramolecular hydrogen bonds also contribute to lower quantum yields, as evidenced by comparing analog compounds SR-1 and SR-3 (**Fig. 2d**, Fig. S60). Our analysis shows that the intramolecular charge transfer from the donor to the acceptor alters the charge density around the amino and oxygen atoms, causing the hydrogen atom to move closer to the oxygen atom in the excited state of SR-1 (Fig. S61). This considerable movement accelerates non-radiative decay and may potentially activate additional non-radiative pathways, such as intersystem crossing and conical intersections, thereby reducing the quantum yield of SR-1.

Significant TICT formation was observed in these single-benzene derivatives (Fig. S65). For example, the pre-twisted SR-2 displays a lower energy barrier and a strong driving force towards TICT (**Fig. 3b**), wherein the -$N(CH_3)_2$ rotates to become perpendicular to the fluorophore scaffold, resulting in complete charge separation and a zero oscillator strength (*f*) (Fig. S66). TICT is typically enhanced in polar solvents due to the strong dipole-dipole interactions between the fluorophore in the TICT state and the surrounding solvent molecules, which help stabilize this state.[19, 43, 44] Consequently, the quantum yield (φ) of SR-2 is generally lower in polar solvents (Table S1).

Transient absorption studies

We further collected transient absorption (TA) spectra of SR-1 and SR-2 in three distinct solvents (*n*-hexane, DMSO, and ethanol) to validate our computational findings of fluorescence quenching channels.

TA spectra corroborate hydrogen bond-induced quenching in SR-1. In non-protic solvents like *n*-hexane (**Fig. 3d**) or DMSO (Fig. S67b), no significant peak shifts were observed in the TA spectra of SR-1. The excited state has a long lifetime, with notable decay starting after >100 picoseconds. In contrast, the TA spectrum of SR-1 in ethanol (polar and protic) shows two excited state absorption (ESA) bands peaking at ~650 and ~660 nm (**Fig. 3e**). About 45 ps after photoexcitation, the first band starts to decay, and the second band emerges, forming an isosbestic point at ~703 nm. This new band decays in ~1.0 ns, close to the fluorescence lifetime (Table S1). We inferred that hydrogen bonding interactions between SR-1 and ethanol molecules stabilize the ICT state, yielding a relaxed ICT state (**Fig. 3e**, Fig. S68c), causing a slight TA spectral peak shift. The stimulated emission (SE) band weakens in this relaxed state, indicating that hydrogen bond-induced vibrations quench the fluorescence. Similar phenomena were observed in SR-5, showing hydrogen bonding sensitivity (Figs. S73, 74).

SR-2 exhibits bright locally excited (LE) emission in *n*-hexane (apolar solvent; **Fig. 3f**). Over time, the ESA peak (~530 nm) shifts slightly while the ESA band at ~650-800 nm narrows, due to the "cooling" of different vibration states in the excited state. Fitting to the LE state shows a decay time of ~15 ns, consistent with the steady-state fluorescence lifetime.

In ethanol, SR-2 shows two ESA bands at ~560 and ~730 nm, with minimal SE signal, aligning with its low fluorescence quantum yield in polar solvents (**Fig. 3g**). The ESA peaks shift over time, indicating the formation of a new excited state (from ICT to TICT; **Fig. 3c** and Fig. S70c). Population profiles show that the decrease in ICT species coincides with the increase in the TICT population. Analysis suggests the ICT to TICT transformation rate is about 18 ps^{-1}. The ICT state decays to the ground state in ~1.4 ns, while the non-emissive TICT state decays in ~500 ps. Similar patterns in SR-3 (Figs. S71, 72), SR-6 (Figs. S75, 76), and SR-7 (Figs. S77, 78) support our computational predictions of TICT quenching channels.

Wash-free super-resolution imaging

The unique environmental sensitivity of the newly developed single-benzene fluorophores provides the potential for wash-free bioimaging applications. We explored the application of these SR dyes in various contexts, focusing mainly on lipid droplets (LDs). As dynamic organelles involved in lipid storage and metabolism, LDs play critical roles in numerous physiological processes. Dysfunction in LDs is linked to diseases, such as fatty liver, diabetes, obesity, cancer, and atherosclerosis.[45] Therefore, studying LD dynamics in live cells is crucial for understanding the underlying mechanisms of these conditions.

Among the SR dyes, SR-6 demonstrated the highest selectivity for lipid droplets despite not having the longest emission wavelength. Co-staining live MCF cells with Hoechst 33342 (a nuclear stain; **Fig. 4a**) and BODIPY 493 (a lipid droplet stain; **Fig. 4d**) revealed excellent colocalization between BODIPY 493 and SR-6 (**Figs. 4c** and **4e**), confirming its specificity. In regions of interest (ROI-1 and ROI-2), SR-6 emitted bright fluorescence within lipid droplets (ROI-1) with minimal cytoplasmic background (ROI-2; **Figs. 4g** and **4h**), resulting in an outstanding signal-to-noise ratio (SNR) of 6.74 $\pm$2.04, which was higher than that of BODIPY 493 (SNR = 4.67$\pm$0.82, Fig. S81). Additionally, SR-6 enabled two-photon fluorescence imaging, with signals that closely overlapped with those from one-photon fluorescence imaging (**Figs. 4i-4l**).

The high photostability of SR-6 further allowed extended imaging of lipid droplets over 1200 seconds under super-resolution imaging. Notably, the calculated logP (ClogP) value (1.92) of SR-6 suggests moderate lipid affinity, indicating that a portion of SR-6 may remain in the cytoplasm.[46] In aqueous environments, these cytoplasmic dyes are non-emissive due to significant quenching. However, they can act as an effective "buffer," slowly diffusing into LDs to replenish photobleached dyes within the LDs. This .

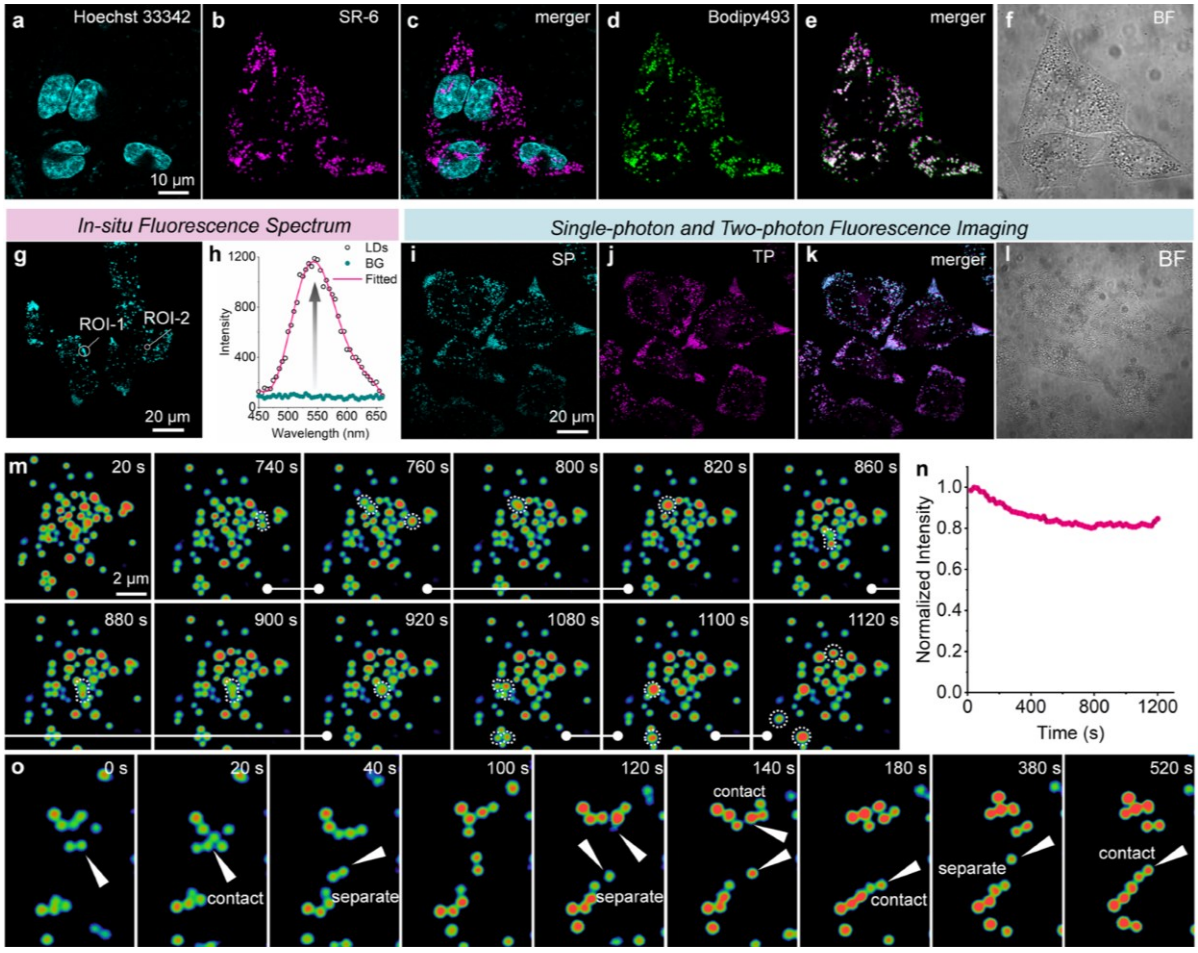

Figure 4. Wash-free imaging of lipid droplets (LDs) in live cells. a, **b**, **d,** Confocal images of Hoechst 33342 (3.0 μM, **a**), SR-6 (20 μM, **b**), and BODIPY 493 (0.5 μM, **d**) in live MCF cells. **c**, The merger of (**a**) and (**b**). **e**, The merger of (**b**) and (**d**). **f**, The bright field image of MCF. Scale bar: 10 μm. **g**, Confocal image of SR-6 (20 μM) in live MCF cells. The two marked areas represent the imaging of lipid droplets (ROI-1) and cytoplasm (ROI-2). **h**, The situ fluorescence spectra of lipid droplets (ROI-1) and cytoplasm (ROI-2). Scale bar: 20 μm. **i-l**, Single-photon (SP), and two-photon (TP) images of lipid droplets in MCF. Scale bar: 20 μm. **m-o**, Super-resolution images of LDs dynamics. Seven LDs-LDs coalescence processes (**m**) were taken separately and marked with white dotted lines. (**n**) Relative intensity changes of SR-6 during LDs super-resolution imaging. (**o**) Dynamic contacting and separating processes of different LDs were observed and marked with white arrows. Scale bar: 2 μm.

replenishment enhances effective photostability, enabling long-term imaging.

During this course, we observed dynamic interactions between lipid droplets, such as coalescence, contact, and separation events (**Figs. 4m** and **4o**). We noted that SR-6 exhibited less than a 20% intensity drop over 1200 seconds of continuous imaging (**Fig. 4n**).

It is worth noting that SR-3 also successfully stained live cells, although their fluorescence intensity was weaker than that of SR-6. This difference is presumably due to the enhanced solubility of SR-3 in aqueous solution, where the dyes are non-emissive (Fig. S79a-c).

As the small size of SR dyes is not essential for LD imaging, we assessed their performance in studying tiny cavities for non-biological applications, where size effects play a critical role. For example, SR-3 (MW = 244 g/mol) and SR-7 (MW = 272 g/mol) could penetrate the small cavities of molecular sieves, enabling three-dimensional visualization of these structures with good photostability (Figs. S83, 84, 86, 87). No fluorescence was observed outside the sieves, as SR dyes remain non-emissive in protic solvents like water. In contrast, the reference compound Coumarin 153 (MW = 309 g/mol) could not enter the sieves, leading to bright emission from the background rather than from the sieves (Fig. S85). These results show that SR dyes offer a powerful tool for the 3D visualization of small cavities.

SR-based amino acid for wash-free imaging of bacterial growth

Next, we synthesized fluorescent unnatural amino acids to further enhance the selectivity and functionality of the SR dyes for targeted bioimaging applications. Fluorescent unnatural amino acids have gained prominence over the last decade as versatile tools for minimally disruptive modification of peptides and proteins.[47, 48] Modular synthetic approaches have been developed to create fluorescent probes from naturally occurring amino acids. These probes offer variable optical properties and have wide-ranging

biological applications.[49] Notably, fluorescent derivatives of D-alanine can be metabolically recognized and incorporated into the peptidoglycans of bacterial cell walls.[50, 51] However, the large size of the fluorophore often causes many artificially synthesized amino acids to lose their intended functionality.[6, 24, 52]

In our study, we aimed to develop a novel SR-based derivative of D-alanine to assess its potential for live-cell imaging, particularly in bacterial cell wall biosynthesis. The spectral

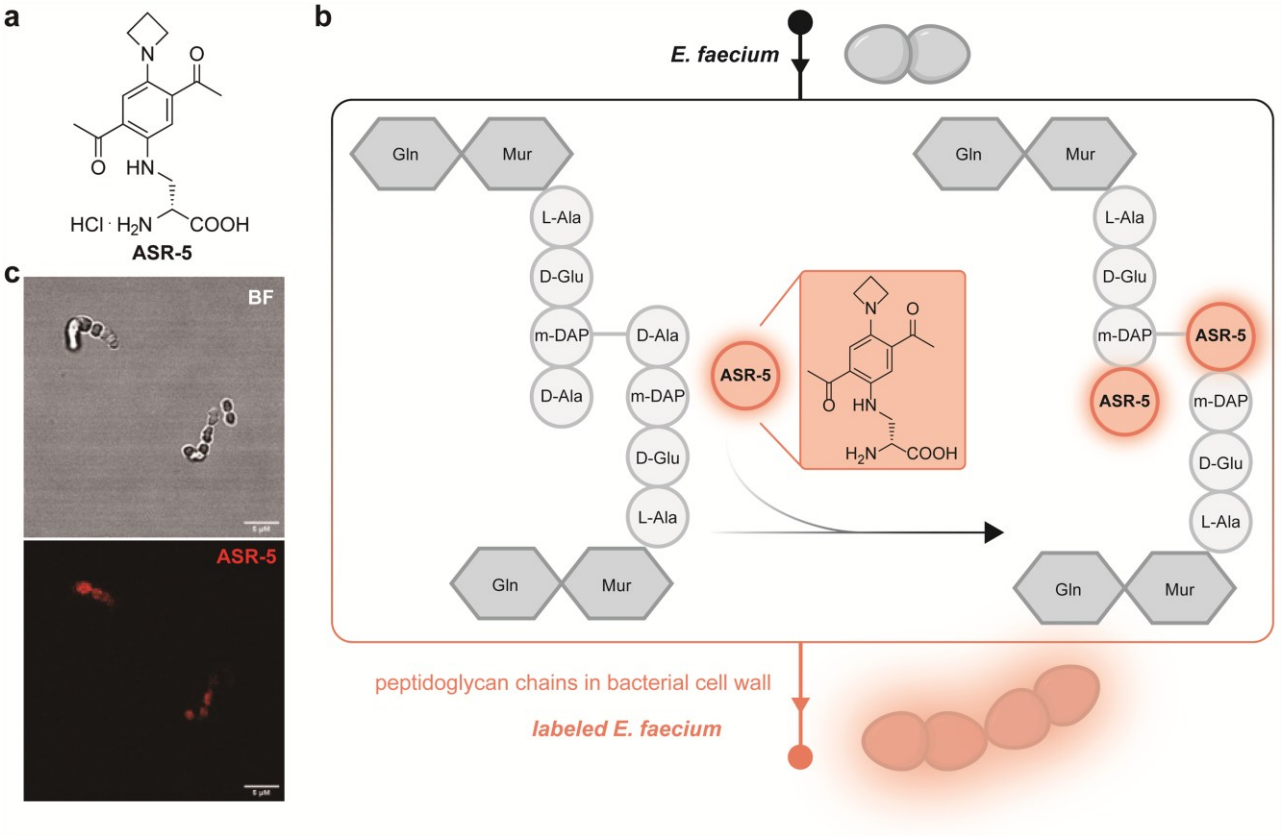

Figure 5. Wash-free imaging of bacterial growth. a, Chemical structure of the fluorogenic amino acid ASR-5. **b**, Schematic illustration of the incorporation of ASR-5 into positions 4 and 5 of the peptidoglycan cell wall during cell wall turnover or division (Gln: N-acetylglucosamine, Mur: N-acetylmuramic acid). **c**, Representative bright field (top and fluorescence (bottom) microscopy images of E. faecium after incubation with compound ASR-5. Images were taken under a fluorescence microscope (ex./em.: 440/500-700 nm) without any washing steps. Scale bars: 5 µm.

analysis confirmed that Boc-ASR-5, a fused analog of SR-5 and SR-7 (Fig. S88), retained the desired optical characteristics (λ_{abs} = 464 nm, λ_{em} = 642 nm in DCM) of the unmodified dyes (Figs. S47, 50, 90). This result validates the suitability of SR fluorophores for conjugation with bioactive molecules, ensuring their effectiveness in biological applications. Subsequent deprotection under mildly acidic conditions yielded ASR-5, an SR-based fluorescent analog of D-alanine.

ASR-5 represents the first example of a fluorescent D-amino acid featuring a single-benzene fluorophore. Its structural similarity to D-alanine suggested that ASR-5 could replace natural D-alanine residues and integrate into positions 4 and 5 of the peptidoglycan chain during bacterial cell wall biosynthesis (**Fig. 5b**). This hypothesis was confirmed by wash-free fluorescence imaging, which demonstrated uniform labeling of *E. faecium* bacterial cells, indicating successful incorporation of ASR-5 into their peptidoglycan chains (**Fig. 5c**). Control experiments, including imaging of cells without ASR-5 and with SR-7 (lacking the D-alanine moiety), showed no fluorescence, further corroborating the specificity of ASR-5 in bacterial labeling (Fig. S92).

CONCLUSION

This study established an iterative design method for developing NIR fluorophores with compact structures. We achieved this goal through the stepwise attachment of two donors and two acceptors at strategic positions on the benzene scaffolds, enhancing push-pull electronic effects and meticulously controlling steric hindrance. These design strategies yielded fluorophores with an emission spectrum extending into the NIR region (>700 nm) and minimal molecular weight (<200 g/mol). Notably, these fluorophores demonstrated remarkable environmental sensitivity, exhibiting intense luminescence in aprotic solvents while undergoing pronounced quenching in aqueous environments. This unique property enabled wash-free bioimaging of lipid droplets in live cells and bacterial growth. While our single-benzene fluorophores require enhancements in molar absorption coefficients, red-shifting UV-vis absorption spectra, and functionalization for specific applications such as

bioimaging and sensing, the adaptability of our design methodology extends to diverse fluorophore scaffolds. This versatility lays the foundation for exploring novel molecules with compact sizes, long wavelengths, expanded functionalities, and broader applications.

ASSOCIATED CONTENT

Supporting Information

The Supporting Information is available free of charge at XX.

Quantum chemical calculations methods, regents, materials, additional experimental details, crystallographic data, ^{1}H and ^{13}C NMR spectra, high-resolution mass spectra, additional calculation results, steady/transient-state optical spectra, and additional bioimaging details

Accession Codes

The structural data for SR fluorophores are freely available from the Cambridge Crystallographic Data Centre. (CCDC no.2381987, 2381988, 2381989, 2381990, 2381991, 2381992, 2381993,[53] 2381994, 2381995 and 2381996 for SR-2 to SR-11, respectively.)

AUTHOR INFORMATION

Corresponding Authors

Xiaogang Liu – Fluorescence Research Group, Singapore University of Technology and Design, 8 Somapah Road, Singapore; ORCID: 0000-0002-2553-2068; E-mail: xiaogang_liu@sutd.edu.sg

Yu Fang – Key Laboratory of Applied Surface and Colloid Chemistry (Ministry of Education), School of Chemistry and Chemical Engineering, Shaanxi Normal University, Xi'an, Shaanxi, China; ORCID: 0000-0001-8490-8080; E-mail: yfang@snnu.edu.cn

Zhaochao Xu – CAS Key Laboratory of Separation Science for Analytical Chemistry, Dalian Institute of Chemical Physics, Chinese Academy of Sciences, 457 Zhongshan Road, Dalian, China; ORCID: 0000-0002-2491-8938; E-mail: zcxu@dicp.ac.cn

Marc Vendrell – Centre for Inflammation Research, The University of Edinburgh, EH16 4UU Edinburgh, the United Kingdom; IRR Chemistry Hub, Institute for Regeneration and Repair, The University of Edinburgh, EH16 4UU Edinburgh, the United Kingdom; ORCID: 0000-0002-5392-9740; E-mail: marc.vendrell@ed.ac.uk

Authors

Rongrong Huang – Fluorescence Research Group, Singapore University of Technology and Design, 8 Somapah Road, Singapore; ORCID: 0000-0001-7341-6953

Qinglong Qiao – CAS Key Laboratory of Separation Science for Analytical Chemistry, Dalian Institute of Chemical Physics, Chinese Academy of Sciences, 457 Zhongshan Road, Dalian, China; ORCID: 0000-0002-2365-5697

Deborah Seah – Centre for Inflammation Research, The University of Edinburgh, EH16 4UU Edinburgh, the United Kingdom; IRR Chemistry Hub, Institute for Regeneration and Repair, The University of Edinburgh, EH16 4UU Edinburgh, the United Kingdom

Tianruo Shen – Fluorescence Research Group, Singapore University of Technology and Design, 8 Somapah Road, Singapore; ORCID: 0000-0001-5417-0783

Xia Wu – Fluorescence Research Group, Singapore University of Technology and Design, 8 Somapah Road, Singapore

Fabio de Moliner – Centre for Inflammation Research, The University of Edinburgh, EH16 4UU Edinburgh, the United Kingdom; IRR Chemistry Hub, Institute for Regeneration and Repair, The University of Edinburgh, EH16 4UU Edinburgh, the United Kingdom

Chao Wang – Fluorescence Research Group, Singapore University of Technology and Design, 8 Somapah Road, Singapore; ORCID: 0000-0003-4981-9335

Nannan Ding – Key Laboratory of Applied Surface and Colloid Chemistry (Ministry of Education), School of Chemistry and Chemical Engineering, Shaanxi Normal University, Xi'an, Shaanxi, China

Weijie Chi – Collaborative Innovation Center of One Health, School of Chemistry and Chemical Engineering, Hainan University, Haikou, Hainan, China; ORCID: 0000-0003-1776-0025

Huaming Sun – Key Laboratory of Applied Surface and Colloid Chemistry (Ministry of Education), School of Chemistry and Chemical Engineering, Shaanxi Normal University, Xi'an, Shaanxi, China; ORCID: 0000-0001-7133-1948

Author Contributions

R.H. and Q.Q. contributed equally.

Notes

The authors declare no competing financial or non-financial interests.

ACKNOWLEDGMENTS

The authors are thankful for the financial support from the Ministry of Education, Singapore (MOE-T2EP10222-0001), the Singapore University of Technology and Design (SUTD) (SKI 2021_04_09), the National Key Research and Development Program of China (2022YFA1205502), the National Natural Science Foundation of China (22132002, 22225806, 22078314, 22278394, 22378385), Dalian Institute of Chemical Physics (DICPI202142, DICP I202227, DICPI202436), the 111 projects (B14041), the Medical Research Council (MR/R01566X/1) and an ERC Consolidator Grant (DYNAFLUORS, 771443). The authors are grateful for the computational resources from SUTD, the National Supercomputing Centre (Singapore), and the transition-state absorption measurement platform at the Institute of New Concept Sensors and Molecular Materials, Shaanxi Normal University. Prof. Jiani Ma, Prof. Jingbai Li, Dr. Davin Tan, and Yangtao Shao are acknowledged for their helpful discussion. Miss Goy Kai Xuan is acknowledged for her assistance with graphic design. R.H. would also like to express gratitude to her soon-to-be-born child, whose presence has been a source of strength and inspiration throughout this process.

REFERENCES

1. Grimm, J. B.; Lavis, L. D., Caveat fluorophore: an insiders' guide to small-molecule fluorescent labels. *Nat. Methods* **2022,** *19* (2), 149-158.

2. Hu, Y.; Yu, J.; Xu, M.; Pu, K., Bienzyme-locked activatable fluorescent probes for specific imaging of tumor-associated mast cells. *J. Am. Chem. Soc*. **2024**, *146* (18), 12656−12663.

3. Jiang, G.; Liu, H.; Liu, H.; Ke, G.; Ren, T. B.; Xiong, B.; Zhang, X. B.; Yuan, L., Chemical approaches to optimize the properties of organic fluorophores for imaging and sensing. *Angew. Chem. Int. Ed.* **2023,** *63* (11), e202315217.

4. Chen, Y.; Wang, S.; Zhang, F., Near-infrared luminescence high-contrast in vivo biomedical imaging. *Nat. Rev. Bioeng.* **2023,** *1* (1), 60-78.

5. Huang, Y.; Chang, M.; Gao, X.; Fang, J.; Ding, W.; Liu, J.; Shen, B.; Zhang, X., NRhFluors: quantitative revealing the interaction between protein homeostasis and mitochondria dysfunction via fluorescence lifetime imaging. *ACS Cent. Sci.* **2024,** *10*, 842−851.

6. Benson, S.; de Moliner, F.; Tipping, W.; Vendrell, M., Miniaturized chemical tags for optical imaging. *Angew. Chem. Int. Ed.* **2022,** *61* (34), e202204788.

7. Yan, K.; Hu, Z.; Yu, P.; He, Z.; Chen, Y.; Chen, J.; Sun, H.; Wang, S.; Zhang, F., Ultra-photostable small-molecule dyes facilitate near-infrared biophotonics. *Nat. Commun.* **2024,** *15* (1), 2593.

8. Balzarotti, F.; Eilers, Y.; Gwosch, K. C.; Arvid H. Gynnå; Westphal, V.; Stefani, F. D.; Elf, J.; Hell, S. W., Nanometer resolution imaging and tracking of fluorescent molecules with minimal photon fluxes. *Science* **2017,** (355), 606-612.

9. Lukinavičius, G.; Umezawa, K.; Olivier, N.; Honigmann, A.; Yang, G.; Plass, T.; Mueller, V.; Reymond, L.; Corrêa Jr, I. R.; Luo, Z.-G.; Schultz, C.; Lemke, E. A.; Heppenstall, P.; Eggeling, C.; Manley, S.; Johnsson, K., A near-infrared fluorophore for live-cell super-resolution microscopy of cellular proteins. *Nat. Chem.* **2013,** *5* (2), 132-139.

10. Vahrmeijer, A. L.; Hutteman, M.; van der Vorst, J. R.; van de Velde, C. J. H.; Frangioni, J. V., Image-guided cancer surgery using near-infrared fluorescence. *Nat. Rev. Clin. Oncol.* **2013,** *10* (9), 507-518.

11. Guo, Z.; Park, S.; Yoon, J.; Shin, I., Recent progress in the development of near-infrared fluorescent probes for bioimaging applications. *Chem. Soc. Rev.* **2014,** *43* (1), 16-29.

12. Wang, F.; Zhong, Y.; Bruns, O.; Liang, Y.; Dai, H., In vivo NIR-II fluorescence imaging for biology and medicine. *Nat. Photon.* **2024,** *18* (6), 535-547.

13. Mc Larney, B. E.; Sonay, A. Y.; Apfelbaum, E.; Mostafa, N.; Monette, S.; Goerzen, D.; Aguirre, N.; Exner, R. M.; Habjan, C.; Isaac, E.; Phung, N. B.; Skubal, M.; Kim, M.; Ogirala, A.; Veach, D.; Heller, D. A.; Grimm, J., A pan-cancer dye for solid-tumour screening, resection and wound monitoring via shortwave and near-infrared fluorescence imaging. *Nat. Biomed. Eng.* **2024**, DOI: 10.1038/s41551-024-01248-w.

14. Dai, M.; Yang, Y. J.; Sarkar, S.; Ahn, K. H., Strategies to convert organic fluorophores into red/near-infrared emitting analogues and their utilization in bioimaging probes. *Chem. Soc. Rev.* **2023,** *52* (18), 6344-6358.

15. Xu, L.; Zhang, Q.; Wang, X.; Lin, W., Biomedical applications of NIR-II organic small molecules fluorescent probes in different organs. *Coord. Chem. Rev.* **2024,** *519*, 216122.

16. Zeng, S.; Liu, X.; Kafuti, Y. S.; Kim, H.; Wang, J.; Peng, X.; Li, H.; Yoon, J., Fluorescent dyes based on rhodamine derivatives for bioimaging and therapeutics: recent progress, challenges, and prospects. *Chem. Soc. Rev.* **2023,** *52* (16), 5607-5651.

17. Xiong, Z.; Zhang, J.; Wang, L.; Liu, X.; Sun, J. Z.; Zhang, H.; Tang, B. Z., Virtual screening for an ultra-small NIR emitter with only two isolated hexatomic rings. *Chem* **2024,** (11), 1-15.

18. Yu, L.; Abbas Abedi, S. A.; Lee, J.; Xu, Y.; Son, S.; Chi, W.; Li, M.; Liu, X.; Park, J. H.; Kim, J. S., Blending low-frequency vibrations and push–pull effects affords superior photoacoustic imaging agents. *Angew. Chem. Int. Ed.* **2023,** *62* (32), e202307797.

19. Liu, X.; Qiao, Q.; Tian, W.; Liu, W.; Chen, J.; Lang, M. J.; Xu, Z., Aziridinyl fluorophores demonstrate bright fluorescence and superior photostability by effectively inhibiting twisted intramolecular charge transfer. *J. Am. Chem. Soc.* **2016,** *138* (22), 6960-6963.

20. Umezawa, K.; Nakamura, Y.; Makino, H.; Citterio, D.; Suzuki, K., Bright, color-tunable fluorescent dyes in the visible-near-infrared region. *J. Am. Chem. Soc.* **2008,** *130* (5), 1550-1551.

21. Chi, W.; Qi, Q.; Lee, R.; Xu, Z.; Liu, X., A unified push–pull Model for understanding the ring-opening mechanism of rhodamine dyes. *J. Phys. Chem. C* **2020,** *124* (6), 3793-3801.

22. Koide, Y.; Urano, Y.; Hanaoka, K.; Terai, T.; Nagano, T., Development of an Si-rhodamine-based far-red to near-infrared fluorescence probe selective for hypochlorous acid and its applications for biological imaging. *J. Am. Chem. Soc.* **2011,** *133* (15), 5680-5682.

23. Chi, W.; Tan, D.; Qiao, Q.; Xu, Z.; Liu, X., Spontaneously blinking rhodamine dyes for single-molecule localization microscopy. *Angew. Chem. Int. Ed.* **2023,** *62* (39), e202306061.

24. Benson, S.; Fernandez, A.; Barth, N. D.; de Moliner, F.; Horrocks, M. H.; Herrington, C. S.; Abad, J. L.; Delgado, A.; Kelly, L.; Chang, Z.; Feng, Y.; Nishiura, M.; Hori, Y.; Kikuchi, K.; Vendrell, M., SCOTfluors: small, conjugatable, orthogonal, and tunable fluorophores for in vivo imaging of cell metabolism. *Angew. Chem. Int. Ed.* **2019,** *58* (21), 6911-6915.

25. Jin, J. H.; An, J. M.; Kim, D.; Lee, S.; Kim, M.; Kim, D., Amino-SBBF (single benzene-based fluorophore) library: its synthesis, photophysical property, and cellular imaging application. *Dyes and Pigm.* **2024,** *221*, 111811.

26. Tuong Ly, K.; Chen-Cheng, R.-W.; Lin, H.-W.; Shiau, Y.-J.; Liu, S.-H.; Chou, P.-T.; Tsao, C.-S.; Huang, Y.-C.; Chi, Y., Near-infrared organic light-emitting diodes with very high external quantum efficiency and radiance. *Nat. Photon.* **2016,** *11* (1), 63-68.

27. Yan, Z. A.; Yin, C.; Tian, H.; Ma, X., Near-infrared room-temperature phosphorescence from monocyclic luminophores. *Angew. Chem. Int. Ed.* **2024**, DOI: 10.1002/anie.202417397.

28. Kim, H.; Kim, Y.; Lee, D., Small is beautiful: electronic origin and synthetic evolution of single-benzene fluorophores. *Acc. Chem. Res.* **2023,** *57* (1), 140-152.

29. Tang, B.; Wang, C.; Wang, Y.; Zhang, H., Efficient red-emissive organic crystals with amplified spontaneous emissions based on a single benzene framework. *Angew. Chem. Int. Ed.* **2017,** *56* (41), 12543-12547.

30. Chatterjee, T.; Mandal, M.; Mardanya, S.; Singh, M.; Saha, A.; Ghosh, S.; Mandal, P. K., *meta*-Fluorophores: an uncharted ocean of opportunities. *Chem. Commun.* **2023,** *59* (97), 14370-14386.

31. Kang, R.; Talamini, L.; D'Este, E.; Estevão, B. M.; De Cola, L.; Klopper, W.; Biedermann, F., Discovery of a size-record breaking green-emissive fluorophore: small, smaller, HINA. *Chem. Sci.* **2021**, *12* (4), 1392-1397.

32. Shimizu, M.; Takeda, Y.; Higashi, M.; Hiyama, T., 1,4-Bis(alkenyl)-2,5-dipiperidinobenzenes: minimal fluorophores exhibiting highly efficient emission in the solid state". *Angew. Chem. Int. Ed.* **2009,** *48* (20), 3653-6.

33. Beppu, T.; Tomiguchi, K.; Masuhara, A.; Pu, Y. J.; Katagiri, H., Single benzene green fluorophore: solid-state emissive, water-soluble, and solvent- and pH-independent fluorescence with large stokes shifts. *Angew. Chem. Int. Ed.* **2015,** *54* (25), 7332-5.

34. Mandal, M.; Chatterjee, T.; Das, A.; Mandal, S.; Sen, A.; Ta, M.; Mandal, P. K., meta-Fluors—a unique way to create a 200 da ultrasmall fluorophore emitting in red with intense stokes/solvatochromic shift: imaging subcellular nanopolarity in live stem cells. *J. Phys. Chem. C* **2019,** *123* (40), 24786-24792.

35. Liu, H.; Yan, S.; Huang, R.; Gao, Z.; Wang, G.; Ding, L.; Fang, Y., Single-benzene-based solvatochromic chromophores: color-tunable and bright fluorescence in the solid and solution states. *Chem. Eur. J.* **2019,** *25* (72), 16732-16739.

36. Xiang, Z.; Wang, Z. Y.; Ren, T. B.; Xu, W.; Liu, Y. P.; Zhang, X. X.; Wu, P.; Yuan, L.; Zhang, X. B., A general strategy for development of a single benzene fluorophore with full-color-tunable, environmentally insensitive, and two-photon solid-state emission. *Chem. Commun.* **2019,** *55* (76), 11462-11465.

37. Kim, H.; Park, W.; Kim, Y.; Filatov, M.; Choi, C. H.; Lee, D., Relief of excited-state antiaromaticity enables the smallest red emitter. *Nat. Commun.* **2021,** *12* (1), 5409.

38. Liu, X.; Cole, J. M.; Xu, Z., Substantial intramolecular charge transfer induces long emission wavelengths and mega stokes shifts in 6-aminocoumarins. *J. Phys. Chem. C* **2017,** *121* (24), 13274-13279.

39. Wu, X.; Tan, D.; Qiao, Q.; Yin, W.; Xu, Z.; Liu, X., Molecular origins of the multi-donor strategy in inducing bathochromic shifts and enlarging Stokes shifts of fluorescent proteins. *Phys. Chem. Chem. Phys.* **2022,** *24* (26), 15937-15944.

40. Li, D.; Shen, T.; Xue, X.; Chen, W.; Tao, W.; Chi, W.; Liu, S. H.; Tan, Y.; Liu, X.; Yin, J., Synergistic effects of multiple rotors and hydrogen-bond interactions lead to sensitive near-infrared viscosity probes for live-cell microscopy. *Sci. China Chem.* **2023,** *66* (8), 2329-2338.

41. Wang, C.; Chi, W.; Qiao, Q.; Tan, D.; Xu, Z.; Liu, X., Twisted intramolecular charge transfer (TICT) and twists beyond TICT: from mechanisms to rational designs of bright and sensitive fluorophores. *Chem. Soc. Rev.* **2021,** *50* (22), 12656-12678.

42. Gao, Y.; Wang, C.; Chi, W.; Liu, X., Molecular origins of heteroatom engineering on the emission wavelength tuning, quantum yield variations and fluorogenicity of NBD-like SCOTfluors. *Chem. Asian J.* **2020,** *15* (23), 4082-4086.

43. Grimm, J. B.; English, B. P.; Chen, J.; Slaughter, J. P.; Zhang, Z.; Revyakin, A.; Patel, R.; Macklin, J. J.; Normanno, D.; Singer, R. H.; Lionnet, T.; Lavis, L. D., A general method to improve fluorophores for live-cell and single-molecule microscopy. *Nat. Methods* **2015,** *12* (3), 244-250.

44. Wang, C.; Qiao, Q.; Chi, W.; Chen, J.; Liu, W.; Tan, D.; McKechnie, S.; Lyu, D.; Jiang, X.-F.; Zhou, W.; Xu, N.; Zhang, Q.; Xu, Z.; Liu, X., Quantitative design of bright fluorophores and AIEgens via the accurate prediction of twisted intramolecular charge transfer (TICT). *Angew. Chem. Int. Ed.* **2020,** *59*, 10160–10172.

45. Gluchowski, N. L.; Becuwe, M.; Walther, T. C.; Farese, R. V., Lipid droplets and liver disease: from basic biology to clinical implications. *Nat. Rev. Gastroenterol. Hepatol* **2017,** *14* (6), 343-355.

46. Chen, J.; Wang, C.; Liu, W.; Qiao, Q.; Qi, H.; Zhou, W.; Xu, N.; Li, J.; Piao, H.; Tan, D.; Liu, X.; Xu, Z., Stable super-resolution imaging of lipid droplet dynamics through a buffer strategy with a hydrogen-bond sensitive fluorogenic probe. *Angew. Chem. Int. Ed*. **2021**, *60*, 25104-25113.

47. Barth, N. D.; Subiros-Funosas, R.; Mendive-Tapia, L.; Duffin, R.; Shields, M. A.; Cartwright, J. A.; Henriques, S. T.; Sot, J.; Goñi, F. M.; Lavilla, R.; Marwick, J. A.; Vermeren, S.; Rossi, A. G.; Egeblad, M.; Dransfield, I.; Vendrell, M., A fluorogenic cyclic peptide for imaging and quantification of drug-induced apoptosis. *Nat. Commun.* **2020,** *11* (1), 4027.

48. Subiros-Funosas, R.; Ho, V. C. L.; Barth, N. D.; Mendive-Tapia, L.; Pappalardo, M.; Barril, X.; Ma, R.; Zhang, C.-B.; Qian, B.-Z.; Sintes, M.; Ghashghaei, O.; Lavilla, R.; Vendrell, M., Fluorogenic Trp(redBODIPY) cyclopeptide targeting keratin 1 for imaging of aggressive carcinomas. *Chem. Sci.* **2020,** *11* (5), 1368-1374.

49. Cheng, Z.; Kuru, E.; Sachdeva, A.; Vendrell, M., Fluorescent amino acids as versatile building blocks for chemical biology. *Nat. Rev. Chem.* **2020,** *4* (6), 275-290.

50. Hsu, Y.-P.; Rittichier, J.; Kuru, E.; Yablonowski, J.; Pasciak, E.; Tekkam, S.; Hall, E.; Murphy, B.; Lee, T. K.; Garner, E. C.; Huang, K. C.; Brun, Y. V.; VanNieuwenhze, M. S., Full color palette of fluorescent-amino acids for in situ labeling of bacterial cell walls. *Chem. Sci.* **2017,** *8* (9), 6313-6321.

51. Kuru, E.; Hughes, H. V.; Brown, P. J.; Hall, E.; Tekkam, S.; Cava, F.; dePedro, M. A.; Brun, Y. V.; VanNieuwenhze, M. S.,

In situ probing of newly synthesized peptidoglycan in live bacteria with fluorescent D-amino acids. *Angew. Chem. Int. Ed.* **2012,** *51* (50), 12519-12523.

52. Lin, L.; Wu, Q.; Song, J.; Du, Y.; Gao, J.; Song, Y.; Wang, W.; Yang, C., Revealing the in vivo growth and division patterns of mouse gut bacteria. *Sci. Adv.* **2020**; *6*, eabb2531.

53. Huang, R.; Tang, B.; Ye, K.; Wang, C.; Zhang, H., Flexible luminescent organic bulk crystal: 2D elasticity toward 3D optical waveguide. *Adv. Opt. Mater*. **2019**, *7*, 1900927.

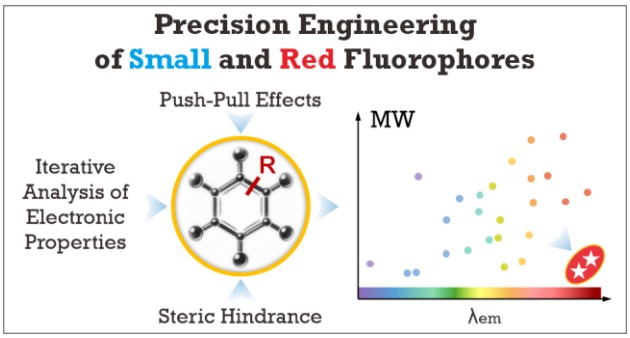

Table of Contents